JOURNAL OF MAGNETIC RESONANCE 93, 151–170 (1991)

Sensitivity Improvement in Proton-Detected Two-Dimensional Heteronuclear Correlation NMR Spectroscopy

ARTHUR G. PALMER III, JOHN CAVANAGH,* PETER E. WRIGHT, AND MARK RANCE

Department of Molecular Biology MB-2, Research Institute of Scripps Clinic, 10666 North Torrey Pines Road, La Jolla, California 92037

Received October 16, 1990

The sensitivity of proton-detected two-dimensional heteronuclear correlation NMR spectroscopy can be increased by as much as a factor of $\sqrt{2}$, relative to that of the conventional methods, for heteronuclei with a single attached proton. The enhanced sensitivity is obtained by refocusing and detecting two orthogonal in-phase proton magnetization components, rather than the single component recorded conventionally. The two magnetization components are deconvoluted to produce two pure-phase spectra that are added together to produce a spectrum with an enhanced signal-to-noise ratio. Methods for improving the sensitivity of the main classes of heteronuclear correlation experiments are presented and the effect of relaxation during the new experiments on the sensitivity enhancement is discussed. The new methods are demonstrated by comparing conventional and sensitivity-enhanced ^{1}H–^{15}N heteronuclear correlation spectra of bovine pancreatic trypsin inhibitor at ^{15}N natural abundance.

NMR spectroscopy is a powerful method for the study of molecular structure and dynamics and increasingly is being used to investigate conformational properties of proteins (*1*). At present, information about the structure of proteins is mostly derived from proton NMR spectroscopy: bond connectivities are characterized by the use of two-dimensional COSY (*2, 3*) and TOCSY (*4*) experiments and interproton distances are determined by the use of two-dimensional NOESY (*5*) experiments. Although this strategy has been fruitful for small proteins, the study of larger proteins by two-dimensional homonuclear NMR techniques is limited in part by the increased resonance overlap in the spectra. Three-dimensional homonuclear NMR has been shown to alleviate some of the overlap problems by offering another dimension into which resonances can be dispersed (*6*). Heteronuclear correlated spectroscopy is another method that has found widespread use in overcoming resonance congestion in two-dimensional homonuclear spectra by means of the larger chemical-shift dispersion of ^{13}C and ^{15}N heteronuclei (*7–9*). Many assignment problems can be simplified by using two-dimensional one-bond heteronuclear correlation spectra in which the two frequency coordinates of a resonance are the chemical shifts of a heteronucleus and

* Present address: Department of Chemistry, University of Cambridge, Lensfield Road, Cambridge CB2 1EW, United Kingdom.

0022-2364/91 $3.00

a proton that are scalar coupled through one bond. The one-bond heteronuclear correlation experiment also is the basis for heteronuclear correlated relay experiments (*10–14*) and for heteronuclear relaxation measurements (*15–17*). To obtain optimum sensitivity in these types of experiments, excitation and detection of proton, rather than heteronuclear, magnetization is required (*8, 9*). The so-called "inverse" detected experiments capitalize on the higher receptivity of protons for detection and give a significant increase in sensitivity compared to experiments in which the heteronucleus is directly detected.

Even with the introduction of proton-detected heteronuclear techniques to increase sensitivity, the biological applications of high-resolution NMR spectroscopy continue to be limited by the desire to study systems that can be obtained only in small quantities or have low solubilities. Consequently, maximizing the inherent sensitivity of any NMR experiment is of paramount importance. An earlier Communication (*18*) demonstrated that the sensitivity of heteronuclear relay spectra, recorded with the heteronuclear single-quantum-coherence technique (HSQC) (*19*) and an isotropic mixing period (*12, 13*), could be increased by up to a factor of $\sqrt{2}$, for heteronuclei with single geminal protons. The sensitivity enhancement was achieved by refocusing two orthogonal in-phase proton magnetization components at the end of the HSQC sequence. In the present paper, methods for recording proton-detected single-bond heteronuclear correlation spectra are described for each of the main classes of heteronuclear correlation experiments that result in similar increases in sensitivity for heteronuclei with single geminal protons. As above, the new procedures derive their sensitivity enhancements from the ability to refocus two orthogonal in-phase proton magnetization components at the end of the various single-bond heteronuclear pulse sequences. A detailed theoretical analysis of the proposed techniques, including a discussion of relaxation effects, is presented, and experimental verification is provided by recording the conventional and sensitivity-enhanced $^{1}H-^{15}N$ correlation spectra of bovine pancreatic trypsin inhibitor (BPTI) at natural ^{15}N abundance. The analysis of the effects of relaxation on the new experiments is also applicable to heteronuclear relay experiments performed by appending isotropic mixing periods to the one-bond correlation experiments (*18*).

THEORY

The extant proton-detected one-bond heteronuclear correlation methods are conveniently categorized according to the form of the density operator after the initial excitation sequence and before the t_1 period. The methods can be classified as follows: (1) sequences in which the operator contains both I and S components that are unmodulated by chemical-shift evolution, (2) sequences in which the operator contains both I and S components that are encoded with the I-spin chemical-shift evolution during the excitation period, and (3) sequences in which the operator contains only S-spin components. The labels I and S refer, respectively, to protons and heteronuclei. Class (1) includes the method of Müller (*20*) and the HSQC sequence (*19*); class (2) includes the HMQC (*21, 22*), Hahndor (*23*), and HSMQC (*24*) sequences; class (3) includes the double DEPT (*9*) and double refocused INEPT (*9*) sequences.

The principle upon which the sensitivity-enhanced sequences are based is broadly applicable; however, the manner in which a given sequence must be amended depends on the particular class of the experiment. Accordingly, the methods of sensitivity enhancement are illustrated for the HSQC, HMQC, and DEPT sequences; the procedures are virtually identical for the other members of the corresponding class. Shown in Fig. 1 are the pulse sequences for (a) HSQC, (b) HMQC, and (c) double DEPT; the corresponding sensitivity-enhanced sequences are shown in Fig. 2. The sensitivity-enhanced proton-detected one-bond heteronuclear correlation methods can be further differentiated depending upon whether the pulse sequences following the t_1 period are based on INEPT (*25*) or DEPT (*21*) polarization transfers. The former group contains experiments based on the HSQC and refocused INEPT sequences; the latter contains experiments based on the HMQC, Hahndor, HSMQC, and double DEPT sequences.

The spin system considered consists of a heteronucleus, denoted the S spin, that has one or more directly attached protons and any number of remotely connected protons, denoted the I spins. All spins are assumed to be weakly coupled and the one-bond heteronuclear scalar coupling between the I and S spins is assumed to be much larger than the homonuclear scalar couplings between attached and remote I spins. The evolution of the density operator during the pulse sequences can be conveniently followed using the product-operator formalism (*26*). In the following, only the product-operator terms that illustrate the principles of the methods are retained; other detectable operator terms are suppressed experimentally by phase cycling, homospoil gradient pulses, or purge pulses. The coefficients of the operator terms are not shown. The effects of the homonuclear scalar coupling between protons are not explicitly considered. Phase errors caused by the evolution of the density operator under the homonuclear scalar coupling terms in the Hamiltonian can be reduced by the addition of purge pulses to the conventional sequences; in the sensitivity-enhanced pulse sequences phase errors are purged by the final pulse on the I spins.

As an example of the principle of sensitivity enhancement, the conventional (Fig. 1a) and improved (Fig. 2a) HSQC experiments are selected because the HSQC experiment is frequently the method of choice for the study of proteins (*27, 28*). The sequence consists of an INEPT polarization transfer from I to S spins, a t_1 evolution period, a reverse INEPT polarization transfer from S to I spins, and a t_2 acquisition period. Beginning with equilibrium I-spin magnetization, the evolution up to the t_1 period is

$$I_z \xrightarrow{90^\circ_x(\mathrm{I})} -I_y \xrightarrow{\Delta-180^\circ_y(\mathrm{I,S})-\Delta} 2I_xS_z \xrightarrow{90^\circ_{-y}(\mathrm{I}),\,90^\circ_x(\mathrm{S})} -2I_zS_y, \quad [1]$$

in which, for example, $90^\circ_x(\mathrm{I})$ represents a pulse with a rotation angle 90° and phase x operating on the I spins, Δ is $1/(4J^{\mathrm{I}}_{\mathrm{IS}})$, and $J^{\mathrm{I}}_{\mathrm{IS}}$ is the one-bond heteronuclear scalar coupling constant. During the t_1 period the antiphase operator evolves solely under the influence of the heteronuclear chemical shift because the 180° pulse on the I spins in the middle of t_1 decouples the I and S spins,

$$-2I_zS_y \xrightarrow{t_1/2-180^\circ_y(\mathrm{I})-t_1/2} 2I_zS_y\cos\omega_{\mathrm{S}}t_1 - 2I_zS_x\sin\omega_{\mathrm{S}}t_1, \quad [2]$$

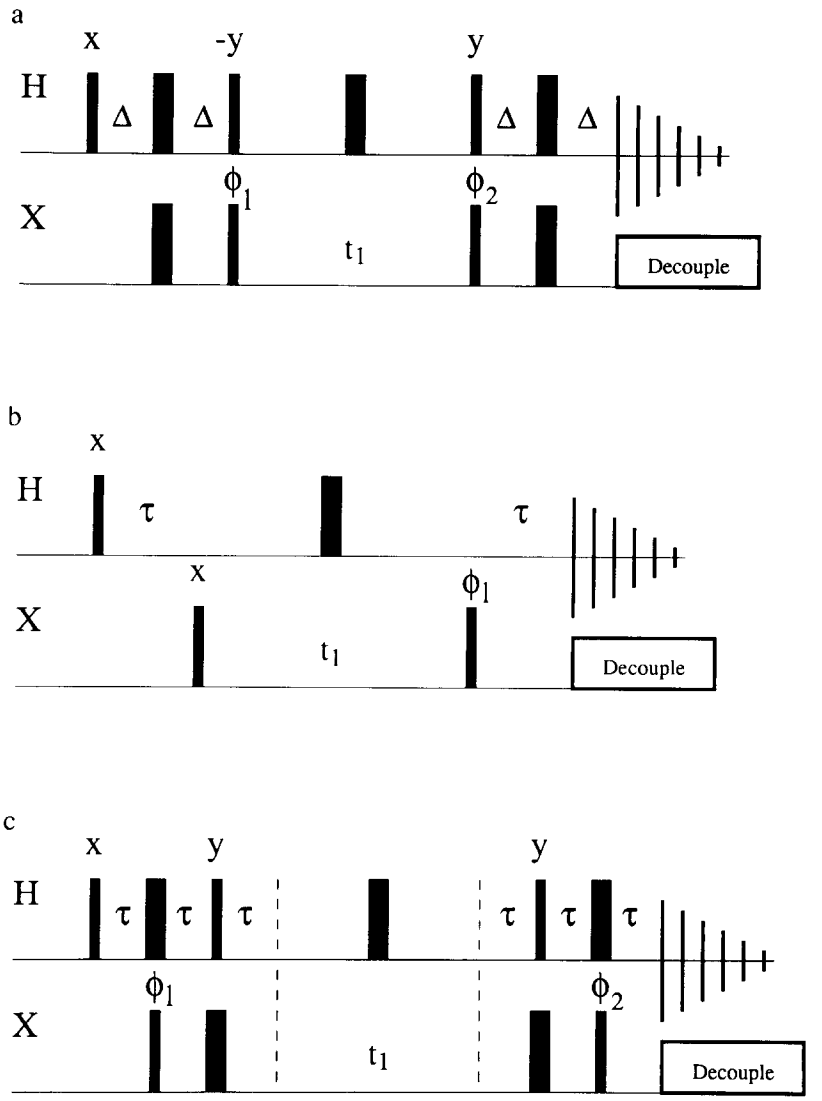

FIG. 1. Pulse sequences for recording conventional heteronuclear correlation spectra. Shown are the pulse sequences for the (a) HSQC, (b) HMQC, and (c) double DEPT methods of acquiring two-dimensional heteronuclear correlation spectra. The thin and thick vertical bars represent 90° and 180° pulses applied to the H (protons) or X (heteronucleus) spins; all 180° pulses in the sequences are applied along the y axis. The delays Δ and τ are $1/(4J^{1}_{HX})$ and $1/(2J^{1}_{HX})$, respectively. Decoupling of the X spins during acquisition is accomplished using the WALTZ-16 (*36*) or other appropriate composite pulse sequence. Quadrature detection in the ω_1 dimension can be achieved by the method of time-proportional phase incrementation (TPPI) (*37*), in which the phase of the 90° pulse on the X spins prior to t_1 is incremented in 90° steps in conjunction with t_1, or by the hypercomplex method (*29, 38*), in which the experiment is performed twice for each t_1 value with the phase of the 90° pulse on the X spins prior to t_1 shifted by 90° between data sets. The basic phase cycling is (a) $\phi_1 = (x\ -x\ x\ -x)$, $\phi_2 = (x\ x\ -x\ -x)$, and receiver = $(x\ -x\ -x\ x)$; (b) $\phi_1 = (x\ -x\ -x\ x)$ and receiver = $(x\ -x\ -x\ x)$; (c) same as (a). The suppression of the magnetization of H spins that are not bound to X spins is improved by using double difference extensions of the basic phase cycle (*39*). In practice composite pulses of the form $90^{\circ}_{x}\ 180^{\circ}_{y}\ 90^{\circ}_{x}$ may be used for the 180° pulses on the X spins. Heteronuclear zero- and double-quantum artifacts can be reduced by phase cycling of the 180° pulse in the middle of the t_1 period. Complete EXORCYCLE phase cycling (*40*) can be used; however, suppression of undesired H magnetization is sometimes superior if the phase of the 180° pulse is simply inverted following the basic phase cycle.

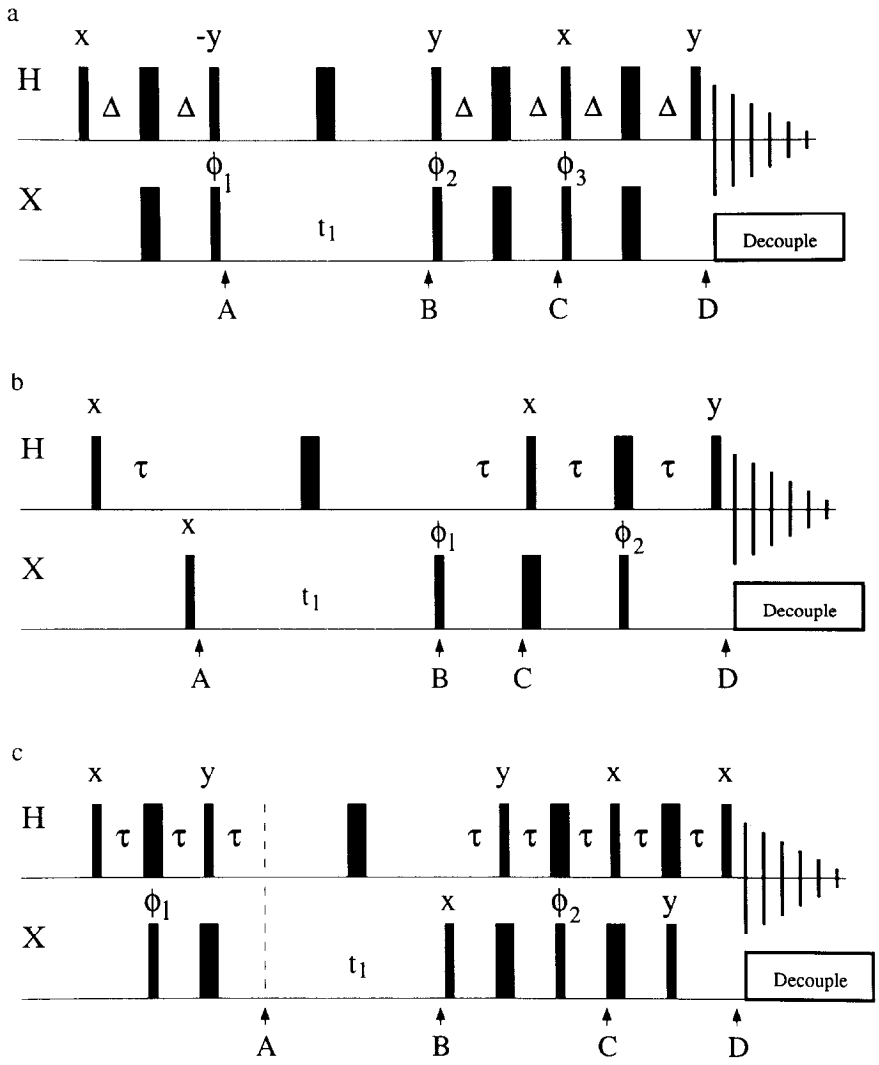

FIG. 2. Pulse sequences for recording heteronuclear correlation spectra with improved sensitivity. Shown are the pulse sequences for improving the sensitivity of the (a) HSQC, (b) HMQC, and (c) double DEPT methods of acquiring two-dimensional heteronuclear correlation spectra. The relevant product operators present at the points labeled A–D in the sequences are given in Table 1. The thin and thick vertical bars represent 90° and 180° pulses applied to the H (protons) or X (heteronucleus) spins; all 180° pulses in the sequences are applied along the y axis. The delays Δ and τ are $1/(4J^{1}_{HX})$ and $1/(2J^{1}_{HX})$, respectively. Decoupling of the X spins is accomplished using the WALTZ-16 or other appropriate composite pulse sequence. Quadrature detection in the ω_1 dimension can be achieved by TPPI or by the hypercomplex method. The basic phase cycling is (a) $\phi_1 = (x\ -x\ x\ -x)$, $\phi_2 = (x\ x\ -x\ -x)$, $\phi_3 = (y\ y\ -y\ -y)$, receiver $= (x\ -x\ -x\ x)$; (b) $\phi_1 = (x\ -x\ -x\ x)$, $\phi_2 = (y\ -y\ -y\ y)$, and receiver $= (x\ -x\ -x\ x)$; and (c) $\phi_1 = (x\ -x\ x\ -x)$, $\phi_2 = (x\ x\ -x\ -x)$, and receiver $= (x\ -x\ -x\ x)$. The suppression of the magnetization of H spins that are not bound to X spins is improved by using double difference extensions of the basic phase cycle. In practice composite pulses of the form $90^{\circ}_{x}\ 180^{\circ}_{y}\ 90^{\circ}_{x}$ may be used for the 180° pulses on the X spins. Heteronuclear zero- and double-quantum artifacts can be reduced by phase cycling of the 180° pulse in the middle of the t_1 period. Complete EXORCYCLE phase cycling can be used; however, suppression of unwanted H magnetization is sometimes superior if the phase of the 180° pulse is simply inverted following the basic phase cycle.

in which ω_S is the Larmor frequency of the decoupled S spins in the rotating reference frame. If the heteronucleus has a single attached proton, the reverse INEPT sequence yields

$$2I_zS_y\cos\omega_S t_1 - 2I_zS_x\sin\omega_S t_1 \xrightarrow{90°_y(I),\ 90°_x(S)} 2I_xS_z\cos\omega_S t_1 - 2I_xS_x\sin\omega_S t_1$$

$$\xrightarrow{\Delta-180°_y(I,\ S)-\Delta} I_y\cos\omega_S t_1 - 2I_xS_x\sin\omega_S t_1. \quad [3]$$

If the heteronucleus has more than one attached proton, evolution of the I_xS_x term under heteronuclear scalar coupling to the passive spins, I′, occurs during the reverse INEPT sequence. For example, if the heteronucleus has two geminal protons then the reverse INEPT sequence yields

$$2I_zS_y\cos\omega_S t_1 - 2I_zS_x\sin\omega_S t_1 \xrightarrow{90°_y(I),\ 90°_x(S)} 2I_xS_z\cos\omega_S t_1 - 2I_xS_x\sin\omega_S t_1$$

$$\xrightarrow{\Delta-180°_y(I,\ S)-\Delta} I_y\cos\omega_S t_1 - 4I_xI'_zS_y\sin\omega_S t_1. \quad [4]$$

In Eqs. [3] and [4], the $I_y\cos\omega_S t_1$ term represents I-spin magnetization that is labeled by the chemical shift of the heteronucleus during t_1 and is detected during t_2. The other terms represent multiple-quantum coherences that are unobservable during t_2; therefore, on average, one-half of the initial I-spin polarization does not contribute to the recorded signal. The resulting two-dimensional data set can be processed into a single-bond heteronuclear correlation spectrum with peak shapes that are purely absorptive in both dimensions.

The evolution of the density operator for the enhanced HSQC sequence proceeds exactly as for the conventional HSQC experiment up to the point labeled C in Fig. 2a, where the operators are given by the final terms in Eqs. [3] and [4]. For a heteronucleus with a single attached proton (Eq. [3]), the evolution through the remainder of the sequence is

$$I_y\cos\omega_S t_1 - 2I_xS_x\sin\omega_S t_1 \xrightarrow{90°_x(I),\ 90°_y(S)} I_z\cos\omega_S t_1 + 2I_xS_z\sin\omega_S t_1$$

$$\xrightarrow{\Delta-180°_y(I,\ S)-\Delta} -I_z\cos\omega_S t_1 + I_y\sin\omega_S t_1$$

$$\xrightarrow{90°_y(I)} -I_x\cos\omega_S t_1 + I_y\sin\omega_S t. \quad [5]$$

The resultant $-I_x\cos\omega_S t_1$ and $I_y\sin\omega_S t$ terms in Eq. [5] describe orthogonal in-phase I-spin magnetization components that have evolved at the frequency of the connected S spin during t_1. Both of these operators are observable during the acquisition period; therefore all of the initial I-spin polarization contributes to the recorded signal. For a heteronucleus with two geminal protons (Eq. [4]), the evolution through the remainder of the sequence is

$$I_y\cos\omega_S t_1 - 4I_xI'_zS_y\sin\omega_S t_1 \xrightarrow{90°_x(\mathrm{I}),\,90°_y(\mathrm{S})} I_z\cos\omega_S t_1 + 4I_xI'_yS_y\sin\omega_S t_1$$

$$\xrightarrow{\Delta-180°_y(\mathrm{I,S})-\Delta} -I_z\cos\omega_S t_1 - 4I_xI'_yS_y\sin\omega_S t_1$$

$$\xrightarrow{90°_y(\mathrm{I})} -I_x\cos\omega_S t_1 + 4I_zI'_yS_y\sin\omega_S t_1. \quad [6]$$

The first term of the resultant in Eq. [6] represents in-phase I-spin magnetization; however, the second term represents unobservable multiple-quantum coherence. As in Eq. [4], only one-half of the initial I-spin polarization is recorded during the acquisition period; consequently, the extended pulse sequences do not provide increased sensitivity for heteronuclei with two geminal protons. Similar considerations hold for heteronuclei with more than two attached protons.

The final two terms in Eq. [5] give rise to superimposed resonances that have a phase difference of 90° in both dimensions of the two-dimensional data set. The two-dimensional spectrum that would result from conventional processing of the data would have peaks with undesirable phase-twisted lineshapes (*29*). To deconvolute the two orthogonal terms and obtain purely absorptive lineshapes, a second experiment is recorded in which the phase of the 90° pulse on the heteronucleus immediately following the t_1 eriod is inverted. Following procedures the same as those used in Eqs. [3] and [5], the operator terms prior to the acquisition period of the second sequence are, beginning with the operators present at the end of Eq. [2],

$$2I_zS_y\cos\omega_S t_1 - 2I_zS_x\sin\omega_S t_1$$

$$\xrightarrow{90°_y(\mathrm{I}),\,90°_x(\mathrm{S})-\Delta-180°_y(\mathrm{I,S})-\Delta-90°_x(\mathrm{I}),\,90°_y(\mathrm{S})-\Delta-180°_y(\mathrm{I,S})-\Delta-90°_y(\mathrm{I})}$$

$$I_x\cos\omega_S t_1 + I_y\sin\omega_S t_1, \quad [7]$$

for a single attached proton. For a heteronucleus with two geminal protons, accumulation of the second experiment yields

$$2I_zS_y\cos\omega_S t_1 - 2I_zS_x\sin\omega_S t_1$$

$$\xrightarrow{90°_y(\mathrm{I}),\,90°_x(\mathrm{S})-\Delta-180°_y(\mathrm{I,S})-\Delta-90°_x(\mathrm{I}),\,90°_y(\mathrm{S})-\Delta-180°_y(\mathrm{I,S})-\Delta-90°_y(\mathrm{I})}$$

$$I_x\cos\omega_S t_1 + 4I_zI'_yS_y\sin\omega_S t_1. \quad [8]$$

Therefore, the observable operators prior to the acquisition period are, for the first experiment,

$$-I_x\cos\omega_S t_1 + \delta_{1,n}I_y\sin\omega_S t_1 \quad [9]$$

and for the second experiment,

$$I_x\cos\omega_S t_1 + \delta_{1,n}I_y\sin\omega_S t_1, \quad [10]$$

in which $\delta_{1,n}$ is the Kronecker delta and n is the number of protons directly attached to the heteronucleus. Addition of the two data sets (Eqs. [9] and [10]) yields the single observable term

$$\delta_{1,n} 2 I_y \sin \omega_S t_1, \qquad [11]$$

while subtraction of the two data sets gives the single observable term

$$-2 I_x \cos \omega_S t_1. \qquad [12]$$

The coefficients of 2 arise in Eqs. [11] and [12] because two acquisitions have been performed. In practice, each of the two data sets required for the enhanced experiment would be acquired with one-half the signal averaging used for the conventional experiment; therefore the entire enhanced and conventional experiments would require the same amount of time to record and the factors of 2 would not appear in the above equations. The data sets described by Eqs. [11] and [12] are identical except for a 90° phase difference in both dimensions and the dependence on the number of attached protons in Eq. [11]; therefore each data set can be transformed and phased into a two-dimensional heteronuclear correlation spectrum with purely absorptive peak shapes in both dimensions. When one neglects relaxation and pulse imperfections in the longer sequences, the spectrum that results from Eq. [12] is identical to the spectrum obtained using the conventional HSQC sequence (Fig. 1a, Eq. [3]). When one neglects relaxation, mismatching between the J_{IS}^{1} constants and the delay Δ, and pulse imperfections, Eq. [11] yields a two-dimensional heteronuclear correlation spectrum that has been edited with a multiplicity filter (*21, 25*). In this spectrum the resonances that arise from heteronuclei with one attached proton have the same intensities as those in the conventional sequence, but the resonances of other heteronuclei are nulled. Thus, two spectra are obtained using the enhanced sequence (Fig. 2a) in the same amount of time required to obtain one spectrum using the conventional sequence (Fig. 1a).

The final spectrum is obtained by adding the two phased spectra obtained from the data sets described by Eqs. [11] and [12]. Applying 90° phase shifts to produce a spectrum with pure absorption peak shapes from the data described by Eq. [11] is identical to performing a two-dimensional Hilbert transform (*30*). Therefore the final spectrum is a linear combination of the original two data sets, described by Eqs. [9] and [10], and their respective Hilbert transforms. As has been shown previously (*30*), the random noise in a spectrum and in its Hilbert transform are statistically independent. Therefore, the noise resulting from spectra acquired and processed in the manner described is statistically independent, and upon addition of the two spectra obtained from Eqs. [11] and [12], the intensities of the resonances of heteronuclei with single attached protons are doubled relative to those in the conventional HSQC spectrum, the intensities of other resonances are unchanged, and the RMS noise is increased by a factor of $\sqrt{2}$. Therefore, the combination of the two spectra described by Eqs. [11] and [12] yields a spectrum in which the overall signal-to-noise ratio increases by $\sqrt{2}$ for heteronuclei with one attached proton.

For the sake of clarity in the above discussion, the procedure for combining the two data sets of Eqs. [11] and [12] in the frequency domain was described; however, the two data sets can also be combined in the time domain if the following two conditions are met. First, the free induction decays must be recorded such that the signals in the quadrature channels are sampled simultaneously rather than alternately in time.

Second, ω_1 frequency discrimination must be achieved via the hypercomplex method rather than by time-proportional phase incrementation (*29*). To combine the two data sets that result from Eqs. [11] and [12] in the time domain, two simple manipulations are performed on one of the data sets: (i) the two quadrature components recorded for each of the FIDs are swapped and the sign of one of the components is inverted, and (ii) the two FIDs recorded for each t_1 value are interchanged and the sign of one of the FIDs is inverted. These two operations correspond to 90° phase shifts in the ω_2 and ω_1 frequency dimensions, respectively. The modified data set is combined with the second, unmodified data set to produce the sensitivity-enhanced data set. Whether the two data sets need to be added or subtracted depends on several factors and is best determined empirically for a given spectrometer; the wrong combination will result in the cancellation of signals. Combining the data in the time domain has the potential advantage that only one data set need be saved, which reduces data storage requirements; in this case, however, the ability to distinguish between IS and I_2S or I_3S spin systems by comparing the spectra arising from the data sets represented by Eqs. [11] and [12] is lost.

The other sensitivity-enhanced sequences shown in Fig. 2 work in virtually the same manner as described for the HSQC sequence. First, the operator that is cosine-modulated during t_1 is transferred to a single-quantum I-spin operator. Second, this operator is stored as longitudinal magnetization while the product operator that is sine-modulated during t_1 is refocused to transverse proton magnetization. Third, the final proton

TABLE 1

Product Operators for Pulse Sequences with Enhanced Sensitivity

Point	HSQC	HMQC	Double DEPT
A	$-2I_zS_y$	$-2I_xS_y\cos\omega_1\tau - 2I_yS_y\sin\omega_1\tau$	S_x
B	$2I_zS_y\cos\omega_S t_1 - 2I_zS_x\sin\omega_S t_1$	$2(I_x\cos\omega_1\tau - I_y\sin\omega_1\tau)(S_y\cos\omega_S t_1 - S_x\sin\omega_S t_1)$	$S_x\cos\omega_S t_1 + S_y\sin\omega_S t_1$
C	$I_y\cos\omega_S t_1 - 2I_xS_x\sin\omega_S t_1$	$I_y\cos\omega_S t_1 - 2I_x\sin\omega_S t_1(S_x\cos\omega_S\tau + S_y\sin\omega_S\tau)$	$-I_y\cos\omega_S t_1 - 2I_z\sin\omega_S t_1(S_x\cos\omega_S\tau + S_y\sin\omega_S\tau)$
D	$-I_x\cos\omega_S t_1 + I_y\sin\omega_S t_1$	$-I_x\cos\omega_S t_1 + I_y\sin\omega_S t_1$	$-I_y\cos\omega_S t_1 - I_x\sin\omega_S t_1$

Note. Shown are the principal product operators, for a heteronuclear S spin with a single geminal proton I spin, that are present at the points labeled A–D in Fig. 2 for the sensitivity-enhanced HSQC, HMQC, and double DEPT pulse sequences. The labels correspond to the endpoints of (A) the initial excitation period, (B) the t_1 evolution period, (C) the coherence transfer and refocusing period for the component that is cosine modulated by the S-spin chemical shift during t_1, and (D) the coherence transfer and refocusing period for the sine-modulated component. The terms at point D are detected during the acquisition period; the sign of one of the components can be negated by inverting the phase of the first 90° pulse on the S spins following the t_1 period in Fig. 2. The Larmor frequencies of the I and S spins are ω_I and ω_S, respectively, $\tau = 1/(2J^1_{IS})$, and the initial operator is I_z. The operators at points A and B are identical to the operators present at the corresponding points in the conventional sequences shown in Fig. 1. The operators at point C are identical to the operators prior to acquisition in the conventional HSQC and HMQC sequences; for the conventional double DEPT sequence, the operator terms are $-I_y\cos\omega_S t_1 - 2I_x\sin\omega_S t_1(S_x\cos\omega_S\tau + S_y\sin\omega_S\tau)$.

90° pulse rotates the longitudinal magnetization back to the transverse plane for acquisition. Other pulses and delays may be necessary to refocus undesirable I- or S-spin chemical-shift evolution during the polarization transfers. In all cases, a second experiment is acquired in which the phase of the first 90° pulse on the heteronuclei after t_1 is inverted and the data are processed as described above. The product operators present at the most informative points in each of the sequences in Fig. 2 are given in Table 1.

The maximum signal-to-noise enhancement of $\sqrt{2}$ is achievable only if relaxation of the density operator during the pulse sequences is negligible. In general, due to additional relaxation during the longer pulse sequences, the magnitudes of the two orthogonal I-spin operators that enter the acquisition period in the enhanced experiments will be less than the magnitudes of the I-spin operators in the conventional experiments. In addition, the magnitudes of the two orthogonal I-spin operators in the enhanced experiments will not be equal because the cosine- and sine-modulated operators present after the t_1 period follow different pathways during the reverse polarization transfers and relax at different rates. Consequently, the sensitivity gains afforded by the proposed methods will be reduced by amounts that depend on both the relative lengths of the conventional and enhanced pulse sequences and the particular product-operator terms that are present during the reverse polarization transfers.

Again, for illustration, the conventional (Fig. 1a) and enhanced (Fig. 2a) HSQC sequences are considered. During the reverse INEPT transfer in the conventional sequence the operator I_xS_z is refocused to I_y (Eq. [3]). The magnitude of the observable operator at the beginning of the t_2 acquisition period is, with the chemical-shift modulation disregarded,

$$I_y = I_y^0 \exp(-2R_{2I}\Delta), \qquad [13]$$

in which R_{2I} is the average of the transverse relaxation rate constants of the in-phase and antiphase I-spin operators and I_y^0 is the magnitude of the operator in the absence of relaxation.

In the enhanced sequence (Eq. [4]), two consecutive reverse INEPT sequences, each of length 2Δ, are used to refocus the heteronuclear operators present after the t_1 period into orthogonal I_x and I_y operators. The magnitude of each of the I_x and I_y operators depends upon the relaxation of the operators present during each of the reverse INEPT sequences. As shown in Eq. [4], the cosine-modulated I_xS_z operator term is refocused to an I_y operator during the first INEPT transfer, stored as I_z magnetization during the second INEPT transfer, and converted to the I_x operator by the final 90° pulse. The relaxation during the first INEPT sequence is described by Eq. [13]. In the second INEPT sequence, the initial I_z operator relaxes toward the thermal-equilibrium polarization during the first delay Δ; then the 180° pulse on the I spins inverts the I_z operator; and finally the I_z operator relaxes from its negated value toward thermal equilibrium during the second delay Δ. The operator, prior to the final pulse of the sequence, is

$$I_z = I_z^\infty - \{2I_z^\infty - [I_z^\infty - I_z^0]\exp(-R_{1I}\Delta)\}\exp(-R_{1I}\Delta), \qquad [14]$$

in which I_z^∞ is the thermal-equilibrium value of the longitudinal magnetization, I_z^0 is

TABLE 2

Effects of Relaxation in Pulse Sequences with Enhanced Sensitivity

	ϵ_a	ϵ_s
HSQC	$\exp(-2R_{2MQ}\Delta)$	$\exp(-2R_{II}\Delta)$
HMQC	$\exp(-2R_{2MQ}\tau)$	$\exp(-2R_{II}\tau)$
DEPT	$\exp(-2R_{IS}\tau)$	$\exp(-2R_{II}\tau)$

Note. Shown are the relative intensities of the two spectra obtained by deconvoluting the two orthogonal magnetization components that are refocused in the sensitivity-enhanced heteronuclear correlation experiments (Fig. 2), compared to the corresponding conventional spectra (Fig. 1). The relative intensities ϵ_a and ϵ_s refer to the spectra, described by Eqs. [11] and [12], that are obtained by the addition and subtraction of the two data sets recorded in the new method. The I-spin longitudinal relaxation rate, the S-spin longitudinal relaxation rate, and the I- and S-spin heteronuclear multiple-quantum relaxation rate are R_{II}, R_{IS}, and R_{2MQ}; Δ and τ are $1/(4J_{IS}^{I})$ and $1/(2J_{IS}^{I})$, respectively. Expressions for the overall improvement in the signal-to-noise ratios of the experiments are obtained using these results in Eq. [24]. Explicit expressions for ϵ_a and ϵ_s can be obtained using Eqs. [25]–[27] for the dipolar relaxation of I and S spins rigidly attached to an isotropically reorienting molecule.

the value of the longitudinal magnetization at the beginning of the second reverse INEPT sequence, and R_{II} is the longitudinal relaxation rate constant for the I spins. Because of the phase cycling of the 90° pulses on the S spins and of the receiver (Fig. 2a), the value of I_z^0 is inverted on alternate scans and the resulting signals are subtracted. The average relaxation of I_z over the phase cycle is found by changing the sign of I_z^0 in Eq. [14] and subtracting the new equation from Eq. [14]:

$$I_z = -I_z^0 \exp(-2R_{II}\Delta). \qquad [15]$$

During the 2Δ delay, cross-relaxation can also occur between I spins which would produce NOESY peaks in the spectrum described by Eq. [12]; however, as Δ is short, any such peaks are expected to be quite weak and difficult to observe. Using Eqs. [13] and [15], following the final pulse of the sequence, the magnitude of the final observable cosine-modulated I_x operator is, with the chemical-shift modulation disregarded,

$$I_x = I_x^0 \exp[-2(R_{2I} + R_{II})\Delta], \qquad [16]$$

in which I_x^0 is the magnitude of the operator in the absence of relaxation. The sine-modulated component following t_1 (Eq. [4]) is stored as I_xS_x multiple-quantum coherence during the first INEPT transfer and refocused from I_xS_z to I_y magnetization during the second INEPT transfer. The magnitude of the final observable operator is, with chemical-shift modulation disregarded,

$$I_y = I_y^0 \exp[-2(R_{2I} + R_{2MQ})\Delta], \qquad [17]$$

in which R_{2MQ} is the average of the transverse relaxation rates of the zero- and double-quantum coherences present during the first INEPT sequence, and I_y^0 is the magnitude of the operator in the absence of relaxation.

The relative intensities of the conventional HSQC spectrum and the spectra that result from addition (Eq. [11]) and subtraction (Eq. [12]) of the two data sets acquired

with the enhanced sequence (Fig. 2a) can be determined from Eqs. [13], [16], and [17]. The relative intensities of the spectra that result from addition and subtraction, compared to the conventional sequence, are

$$\epsilon_a = \exp(-2R_{2MQ}\Delta) \quad [18]$$

and

$$\epsilon_s = \exp(-2R_{11}\Delta), \quad [19]$$

respectively. The relative intensity of the added spectrum, compared to the subtracted spectrum, is

$$\epsilon_r = \epsilon_a/\epsilon_s; \quad [20]$$

since R_{2MQ} will generally be greater than R_{11}, $\epsilon_r < 1$. The achievable sensitivity enhancement is

$$\epsilon = \sqrt{2}(\epsilon_a + \epsilon_s)/2, \quad [21]$$

compared to the maximum value of $\sqrt{2}$.

The analysis of the effects of relaxation of the other sensitivity-enhanced pulse sequences follows similar lines. The results for the relative intensities of the two independent, deconvoluted data sets are given in Table 2.

To estimate the expected sensitivity enhancement for a given molecule, the appropriate relaxation rates, given in Eqs. [18] and [19] and Table 2, must be measured experimentally or calculated for a specific relaxation mechanism. In the following, the I and S spins are assumed to relax solely by dipole–dipole interactions and the spins are assumed to be rigidly attached to a molecule that undergoes isotropic rotational diffusion with a correlation time τ_c. The S spins relax only through interactions with the directly attached I spins; the I spins relax through interactions both with the S spins and with other nearby I spins. Other relaxation mechanisms, such as chemical exchange, scalar relaxation, and chemical-shift anisotropy, are not considered. The I spins are assumed to be in the slow-motion limit with $\omega_I\tau_c \gg 1$ and $\omega_I \gg \omega_S$, where ω_I and ω_S are the Larmor frequencies of the I and S spins, respectively.

The expressions for the dipolar relaxation rate constants for the longitudinal I_z and S_z operators and for the transverse multiple-quantum operator are given by (*31, 32*)

$$R_{11} = \frac{1}{10} D_{IS}^2\{J(\omega_I - \omega_S) + 3J(\omega_I) + 6J(\omega_I + \omega_S)\} + \frac{1}{10}\sum_K D_{IK}^2\{J(0) + 3J(\omega_I) + 6J(2\omega_I)\} \quad [22]$$

$$R_{1S} = \frac{1}{10} D_{IS}^2\{J(\omega_I - \omega_S) + 3J(\omega_S) + 6J(\omega_I + \omega_S)\} \quad [23]$$

$$R_{2MQ} = \frac{1}{20} D_{IS}^2 \{J(\omega_I - \omega_S) + 3J(\omega_I) + 3J(\omega_S) + 6J(\omega_I + \omega_S)\}$$

$$+ \frac{1}{20} \sum_K D_{IK}^2 \{5J(0) + 9J(\omega_I) + 6J(2\omega_I)\}, \quad [24]$$

in which $D_{IJ} = h\gamma_I\gamma_J\mu_0/(8\pi^2 r_{IJ}^3)$, $J(\omega) = \tau_c/(1 + \omega^2\tau_c^2)$, h is Planck's constant, γ_I and γ_J are the gyromagnetic ratios of the I and J spins, r_{IJ} is the length of the internuclear vector between the I and J spins, and μ_0 is the permeability of free space. The summation $\sum_K$ includes all of the homonuclear K $\neq$ I (proton) spins. The longitudinal relaxation rate constant of the S spins, R_{1S}, is required for the analysis of the double DEPT sequence (Table 2). In Eqs. [22]–[24], the terms containing D_{IS} arise from the heteronuclear dipolar coupling between the I and S spins, and the terms containing D_{IK} reflect the homonuclear dipolar coupling between I spins.

In the limit of slow overall tumbling, $J(0) > J(\omega_S) \gg J(\omega_I)$; therefore the relaxation rate constants are approximately given by

$$R_{1I} = D_{IS}^2 J(\omega_I) + \frac{1}{10} J(0) \sum_K D_{IK}^2 \quad [25]$$

$$R_{1S} = \frac{3}{10} D_{IS}^2 J(\omega_S) \quad [26]$$

$$R_{2MQ} = \frac{3}{20} D_{IS}^2 J(\omega_S) + \frac{1}{4} J(0) \sum_K D_{IK}^2. \quad [27]$$

As noted elsewhere (*7, 33*), the expressions for the heteronuclear dipolar contribution to R_{2MQ} in Eqs. [24] and [27] do not depend on $J(0)$ and hence vanish as $\tau_c \rightarrow \infty$; nonetheless, R_{2MQ} can still be considerable because the magnitudes of the homonuclear dipolar terms increase monotonically with τ_c. Typically, for protonated macromolecules with $\omega_S\tau_c \gg 1$, $R_{2MQ} > R_{1I} > R_{1S}$. Applying this inequality to the results in Table 2 indicates that the attainable sensitivity enhancement is greatest for the double DEPT, intermediate for the HSQC, and smallest for the HMQC enhanced sequences, compared to the conventional sequences. Although the enhanced DEPT sequence theoretically has the largest relative sensitivity enhancement, the DEPT sequence is considerably longer than the HSQC and HMQC sequences and may not have a higher absolute sensitivity than these sequences.

Using Eqs. [25] and [27] in Eqs. [18] and [19] yields

$$\epsilon_a = \exp\left\{-2\Delta\left[\frac{3}{20} D_{IS}^2 J(\omega_S) + \frac{1}{4} J(0) \sum_K D_{IK}^2\right]\right\} \quad [28]$$

$$\epsilon_s = \exp\left\{-2\Delta\left[D_{IS}^2 J(\omega_I) + \frac{1}{10} J(0) \sum_K D_{IK}^2\right]\right\}. \quad [29]$$

Similar expressions for the other sequences can be obtained by substituting Eqs. [25]–[27] into the results given in Table 2. The expressions for ϵ_a and ϵ_s for the sensitivity-enhanced sequences are dominated by the term

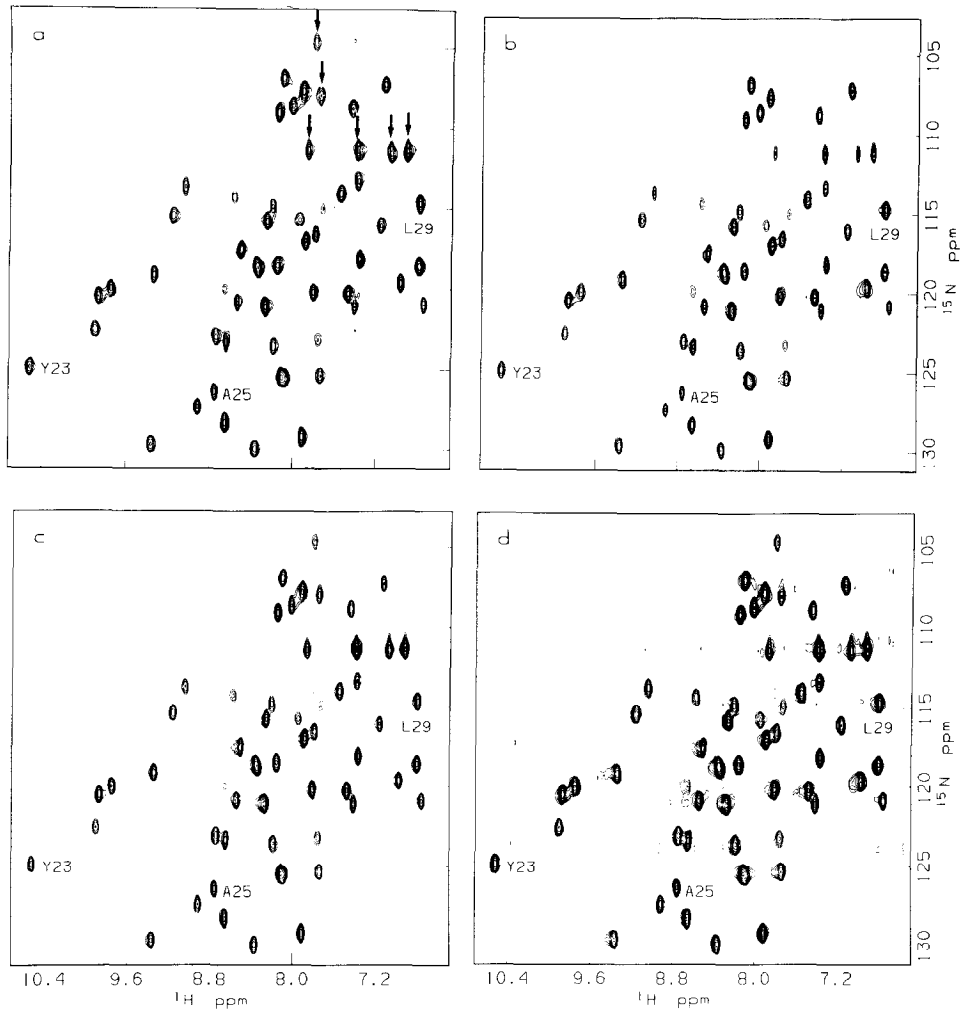

FIG. 3. Contour plots of two-dimensional ^{1}H-^{15}N HSQC spectra of BPTI acquired using conventional and sensitivity-enhanced methods. All experiments were performed on a sample of BPTI (20 mM, 90% H_2O/10% D_2O, pH 4.6, T = 308 K) at natural ^{15}N abundance. Spectroscopy was performed on a Bruker AM500 spectrometer equipped with 451 MHz IF electronics. Data processing was performed using software provided by Dr. Dennis Hare. A conventional HSQC spectrum was acquired using the pulse sequence of Fig. 1a. For this experiment 1024 scans were acquired per t_1 increment. The two data sets required to produce the sensitivity-enhanced HSQC spectrum (pulse sequence of Fig. 2a) were acquired with 512 scans per t_1 increment. For all spectra, 4K real data points (2K per quadrature channel) were acquired in t_2 and 100 real points were acquired in t_1. TPPI was used for frequency discrimination in ω_1. The spectral width was 7042 Hz in ω_2 and 2500 Hz in ω_1. The ^{1}H carrier was placed on the H_2O resonance and the ^{15}N carrier was placed at 108 ppm. The ^{15}N chemical shifts were indirectly referenced from the ^{1}H resonant frequency of the H_2O (*41*). The delay, Δ, was set to 2.3 ms, which is slightly less than $1/(4J^{1}_{HN})$, to reduce relaxation losses. To improve the suppression of magnetization from protons not bound to ^{15}N, a homospoil gradient pulse of 3 ms was applied directly after the second 90° proton pulse. The gradient pulse was followed by a 7 ms delay to allow the magnetic field to stabilize prior to the first 90° heteronucleus pulse. The two data sets acquired using the sequence of Fig. 2a were added and subtracted to produce two new data sets called,

$$J(0) \sum_K D_{IK}^2 = [h\gamma_I^2\mu_0/(8\pi^2)]^2\tau_c \sum_K r_{IK}^{-6} \quad [30]$$

for large proteins with long rotational correlation times. In the absence of significant internal motions, the largest molecules for which the longer sensitivity-enhanced HSQC sequence will yield appreciable gains in the signal-to-noise ratio of the heteronuclear correlation spectra are determined by the values of the parameters in Eq. [30]. Using a typical value of $\Sigma_K r_{IK}^{-6} = 0.027 \pm 0.009$ Å^{-6} for the distances from a backbone proton to the other protons in proteins,[1] enhancement factors $\epsilon > 1.1$ are estimated to be obtainable for molecules with $\tau_c < 20$ ns. The other parameters in Eq. [30] are $h = 6.626 \times 10^{-34}$ J s, $\gamma_I = \gamma_H = 2.6753 \times 10^8$ s^{-1} T^{-1}, and $\mu_0 = 4\pi \times 10^{-7}$ T m/A.

EXPERIMENTAL VERIFICATION

In the study of proteins, sensitivity-enhanced heteronuclear correlation experiments are most useful for correlating the backbone α-carbons or amide nitrogens with their attached protons. Except for the α-carbon of glycine, the imino nitrogen of proline, and the *N*-terminal amide, these heteronuclei all have a single geminal proton, as required for sensitivity enhancement. In addition, the multiplicity-filtered spectrum that is also obtained in these experiments assists in distinguishing backbone resonances from side-chain resonances with similar chemical shifts.

The sensitivity gains predicted theoretically were verified experimentally by the acquisition of two-dimensional heteronuclear correlation spectra using the conventional HSQC pulse sequence (Fig. 1a) and the corresponding sensitivity-enhanced sequence

[1] The average value of $\Sigma_K r_{IK}^{-6}$ was calculated from the atomic coordinates of the zinc finger Xfin-31, BPTI, french bean plastocyanin, and sperm whale myoglobin obtained from the Protein Data Bank (Brookhaven). Distances were calculated from each backbone amide or α proton, except for the α protons of glycines, to the other protons in the protein and the summation executed. The values for the backbone protons were then averaged and the standard deviation calculated. The results can be used to calculate relaxation rates for backbone protons of typical rigid globular proteins.

---

respectively, "ADD" and "SUBTRACT," which were used for subsequent data reduction. Spectra were processed using 8 Hz exponential line broadening in ω_2 and a Kaiser window in ω_1. Spectra were zero filled before Fourier transformation to yield a final size of 2048 real points in each dimension. Shown are (a) the conventional HSQC spectrum, (b) the ADD spectrum, and (c) the SUBTRACT spectrum. The SUBTRACT spectrum was initially phased to be in pure absorption in both dimensions; the ADD spectrum was also phased to be in pure absorption by adding a 90° phase shift in both dimensions relative to the SUBTRACT spectrum. The ADD and SUBTRACT spectra were then added to produce the ENHANCED spectrum shown in (d). All two-dimensional plots are shown on the same absolute scale. Arrows in (a) indicate resonances arising from side-chain groups as noted in the text. The conventional and SUBTRACT spectra are virtually identical, while the ADD spectrum exhibits attenuated resonances in some regions (those indicated by arrows in (a)) due to the multiplicity filter. The assignments of the resonances of Tyr^{23}, Ala^{25}, and Leu^{29} (*42*) are indicated for comparison with Fig. 4. For the 49 backbone amide resonances identified, the ENHANCED HSQC spectrum displays a 1.32 sensitivity improvement over the conventional HSQC spectrum.

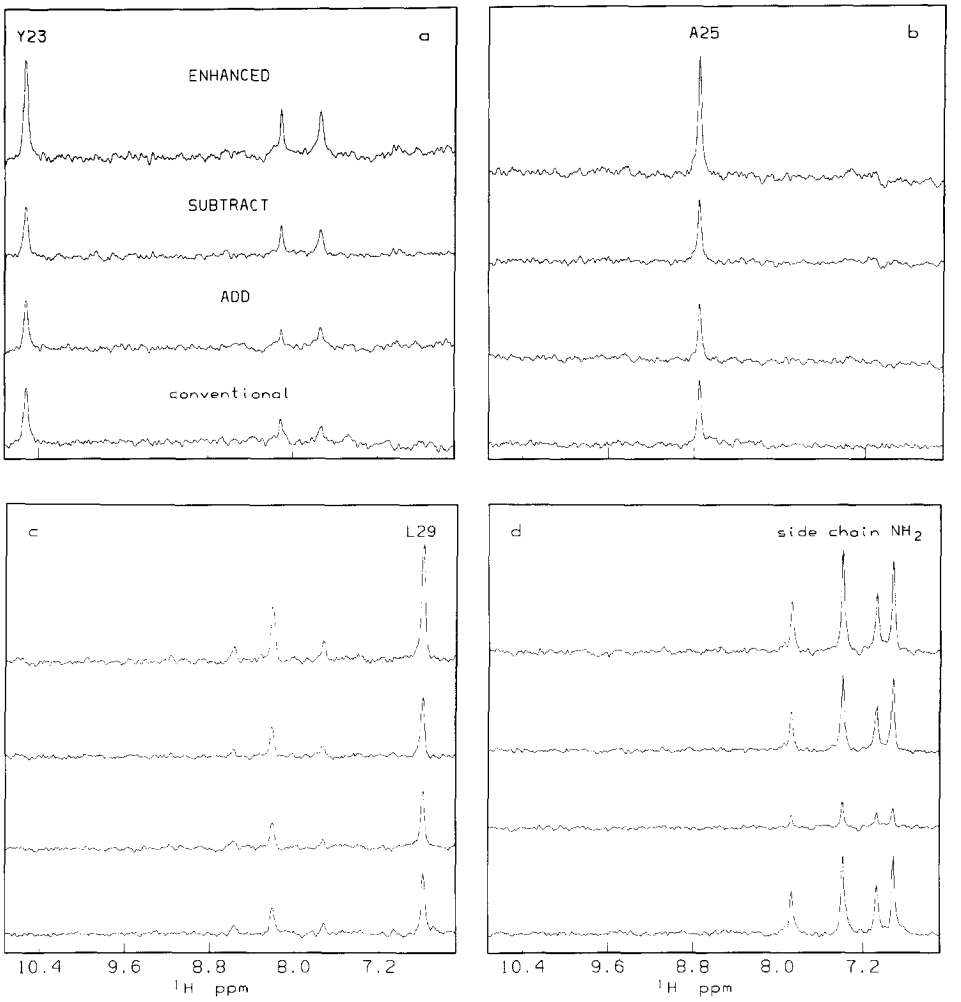

FIG. 4. Cross sections taken parallel to the ω_2 axis, through selected N–H resonances, from the two-dimensional spectra shown in Fig. 3. Cross sections are shown for the amide resonances of (a) Tyr^{23}, (b) Ala^{25}, and (c) Leu^{29}. The NH_2 resonances with a ^{15}N chemical shift of 115 ppm, indicated by arrows in Fig. 3a, are also shown. In each case the bottom trace is taken from the conventional HSQC spectrum, the second trace from the ADD spectrum, the third trace from the SUBTRACT spectrum, and the top trace from the ENHANCED spectrum. The slices are plotted on an absolute intensity scale. In each case the sensitivity improvement of the ENHANCED spectrum over the conventional spectrum is clear and has been measured for the respective examples as (a) 1.26, (b) 1.31, and (c) 1.36. The slices in (d) illustrate the effect of the multiplicity filter of the ADD spectrum. In the conventional HSQC and SUBTRACT spectra, four peaks are visible, corresponding to two NH_2 groups, but these resonances have been suppressed in the ADD spectrum.

(Fig. 2a). The relevant phase-cycling schemes are given in the figure captions to Figs. 1 and 2. All experiments were performed on a sample of the small globular protein BPTI (MW = 6500) at ^{15}N natural abundance. The experimental protocol is given in the caption to Fig. 3. The total acquisition time was 20 hours for the conventional HSQC and 20 hours for the sensitivity-enhanced HSQC experiment. A contour plot of the conventional one-bond HSQC correlation spectrum is shown in Fig. 3a. The two data sets acquired in the sensitivity-enhanced experiment are independent combinations of two orthogonal in-phase proton magnetization components, which, if processed conventionally, would generate spectra with unacceptable phase-twisted lineshapes. To deconvolute the two magnetization components, the two data sets were added to produce a new data set labeled "ADD" and subtracted to produce a second new data set labeled "SUBTRACT." Following two-dimensional Fourier transformation and appropriate phasing, two pure absorption HSQC correlation spectra are obtained; these spectra are shown in Fig. 3b for the ADD spectrum and Fig. 3c for the SUBTRACT spectrum. The sensitivity-enhanced HSQC spectrum is produced by adding the ADD and SUBTRACT spectra. This spectrum is shown in Fig. 3d and is labeled "ENHANCED." Relevant processing parameters are given in the figure caption. For comparison purposes, cross sections taken parallel to the ω_2 dimension from the conventional HSQC, ADD, SUBTRACT, and ENHANCED spectra are shown in Fig. 4 for selected heteronuclear resonances.

On close inspection of the two-dimensional spectra (Fig. 3) and the cross sections (Fig. 4), the SUBTRACT spectrum and conventional HSQC spectrum are virtually identical; however, some resonances in the ADD spectrum exhibit drastically reduced intensities compared to those of either the conventional HSQC or the SUBTRACT spectra. These resonances, indicated by arrows in Fig. 3a, were identified, using a conventional double refocused INEPT experiment (*9*), as side-chain NH_2 groups (data not shown). As noted above, NH_2 resonances are suppressed in the ADD spectrum because only NH resonances are retained by the multiplicity filter implicit in the sensitivity-enhanced sequences. In principle these peaks should be completely absent in the ADD spectrum, but due to mismatching of the Δ delays and the J^1_{NH} coupling, small residual components may remain. An example of the suppression of NH_2 resonances in the ADD spectrum is shown in Fig. 4d. The ability to distinguish side-chain NH_2 groups within one experiment, by comparing ADD and SUBTRACT spectra, is a useful adjunct to this experiment.

As discussed theoretically, the ideal sensitivity enhancement of $\sqrt{2}$ depends upon the statistical independence of the noise in the ADD and SUBTRACT spectra, and the achievable sensitivity enhancement depends on the longitudinal and multiple-quantum relaxation rates of the I and S spins. For the conventional HSQC spectrum, and the ADD, SUBTRACT, and ENHANCED spectra, the magnitudes of the RMS baseline noise were calculated and the intensities of 49 resolved amide peaks were determined. The levels of the RMS noise in the conventional HSQC spectrum, the ADD spectrum, and the SUBTRACT spectrum were nearly identical. The ratio of the RMS noise in the ENHANCED spectrum to that in the conventional spectrum was 1.35, in agreement with the expected value of $\sqrt{2}$. For each amide peak, the values of ϵ_a, ϵ_s, and ϵ were calculated as the ratios of the intensities of the resonance in the

ADD, SUBTRACT, and ENHANCED spectra relative to the intensity in the conventional HSQC spectrum, respectively. As can be clearly seen, a substantial sensitivity improvement is evident from the cross sections shown in Fig. 4; the relative intensities and signal-to-noise enhancement are given for these selected resonances in the figure caption. The average values for all 49 resonances were $\epsilon_a = 0.88 \pm 0.09$, $\epsilon_s = 0.99 \pm 0.07$, and $\epsilon_r = 0.89 \pm 0.08$. The average improvement in the signal-to-noise ratio in the ENHANCED spectrum compared to that in the conventional HSQC spectrum was $\epsilon = 1.32 \pm 0.10$ on the basis of the theoretical increase in the RMS noise. Uncertainties indicated are the standard deviations of the values determined for the 49 resonances.

In accordance with the analysis of the effects of relaxation on the longer enhanced pulse sequences, the overall sensitivity enhancement obtained for the $^1H-^{15}N$ heteronuclear correlation spectra of BPTI was slightly less than $\sqrt{2}$ and ϵ_a, ϵ_s, and ϵ_r were less than unity. Theoretical values of $\epsilon_a = 0.92$, $\epsilon_s = 0.97$, and $\epsilon = 1.34$ were estimated for BPTI using Eqs. [21] and [28]–[30] and $\tau_c = 4$ ns (*34*). The correspondence between the empirical and calculated values suggests that pulse imperfections and evolution of homonuclear scalar couplings are not significantly reducing the signal intensity in the enhanced sequences compared to that in the conventional sequences. In principle, amide proton exchange could also diminish the observed sensitivity enhancements; however, no correlation was observed between resonances having below-average enhancements and amides that have been reported to undergo rapid exchange in BPTI (*35*).

CONCLUSION

A new approach for increasing the sensitivity of heteronuclear correlation spectra for heteronuclei with one geminal proton that is applicable to the existing proton-detected one-bond heteronuclear correlation experiments has been demonstrated. The improved sensitivity results from refocusing and recording two orthogonal in-phase proton magnetization components that can be deconvoluted to generate two pure-phase spectra. One of the two spectra is a conventional heteronuclear correlation spectrum and the other is a multiplicity-filtered spectrum in which only the resonances from heteronuclei with a single geminal proton appear. Addition of these two spectra produces a spectrum with enhanced signal-to-noise ratios for the resonances of heteronuclei with one attached proton because the random noise present in the spectra following deconvolution is statistically independent. A second benefit of the new pulse sequence is that comparison of the two spectra obtained following deconvolution distinguishes heteronuclei with a single geminal proton from other heteronuclei; this can be very useful in studies of backbone heteronuclei in proteins. The new methods have been experimentally verified by comparing conventional and sensitivity-enhanced $^1H-^{15}N$ heteronuclear correlation spectra of BPTI at ^{15}N natural abundance.

The overall sensitivity enhancements attained by the new methods are expected to be slightly less than the ideal factor of $\sqrt{2}$ because the new pulse sequences are longer than the conventional ones and additional relaxation losses occur. In addition, the intensities of corresponding resonances in the two deconvoluted spectra are not identical because the two orthogonal magnetization components travel distinct pathways prior

to acquisition and relax differentially. The theoretical analysis of the effects of relaxation in the new methods agrees with the empirical results from the spectra of BPTI and indicates that the sensitivity-enhanced methods are applicable to proteins of sizes amenable to two-dimensional NMR spectroscopy.

Although the experimental demonstration of the new method has utilized the HSQC sequence, the sensitivity-enhancement procedure described here can be used in conjunction with other proton-detected heteronuclear correlation experiments. Indeed this procedure has been used for sensitivity enhancement of HMQC (Fig. 2b) and double DEPT (Fig. 2c) $^{1}H-^{13}C$ heteronuclear correlation spectra of the zinc finger Xfin-31 with gains in sensitivity similar to those for the HSQC sequence (data not shown).

With the enormous interest in the proton assignments and three-dimensional structures of proteins, possibly the most useful applications of the sensitivity-enhanced heteronuclear correlation experiments correlate backbone amide N–H or α C–H pairs. The increased sensitivity of the new methods may be particularly valuable for measurements of backbone heteronuclear relaxation rates using refocused INEPT or double DEPT experiments. The same principles described herein for the one-bond heteronuclear correlation experiments have been used to improve the sensitivity of two-dimensional heteronuclear relay experiments (*18*).

ACKNOWLEDGMENTS

This material is based upon work supported by the National Science Foundation under a grant (CHE-8907510) awarded in 1989 (A.G.P.) and by grants from the National Institutes of Health (GM 40089 and GM 34663).

REFERENCES

1. K. WÜTHRICH, "NMR of Proteins and Nucleic Acids," Wiley, New York, 1986.
2. J. JEENER, Ampere International Summer School, Basko Polje, Yugoslavia, 1971.
3. W. P. AUE, E. BARTHOLDI, AND R. R. ERNST, *J. Chem. Phys.* **64,** 2229 (1976).
4. L. BRAUNSCHWEILER AND R. R. ERNST, *J. Magn. Reson.* **53,** 521 (1983).
5. J. JEENER, B. H. MEIER, P. BACHMANN, AND R. R. ERNST, *J. Chem. Phys.* **71,** 4546 (1979).
6. C. GRIESINGER, O. W. SØRENSEN, AND R. R. ERNST, *J. Magn. Reson.* **84,** 14 (1989).
7. R. H. GRIFFEY AND A. G. REDFIELD, *Q. Rev. Biophys.* **19,** 51 (1987).
8. A. BAX, S. W. SPARKS, AND D. A. TORCHIA, *in* "Methods in Enzymology" (N. Oppenheimer and T. L. James, Eds.), Vol. 176, pp. 134–150, Academic Press, San Diego, 1989.
9. G. WAGNER, *in* "Methods in Enzymology" (N. Oppenheimer and T. L. James, Eds.), Vol. 176, pp. 93–114, Academic Press, San Diego, 1989.
10. P. H. BOLTON, *J. Magn. Reson.* **48,** 336 (1982).
11. P. H. BOLTON, *J. Magn. Reson.* **62,** 143 (1985).
12. A. BAX, D. G. DAVIS, AND S. K. SARKAR, *J. Magn. Reson.* **63,** 230 (1985).
13. L. LERNER AND A. BAX, *J. Magn. Reson.* **69,** 375 (1986).
14. M. RANCE, P. E. WRIGHT, B. A. MESSERLE, AND L. D. FIELD, *J. Am. Chem. Soc.* **109,** 1591 (1987).
15. N. R. NIRMALA AND G. WAGNER, *J. Am. Chem. Soc.* **110,** 7557 (1988).
16. N. R. NIRMALA AND G. WAGNER, *J. Magn. Reson.* **82,** 659 (1989).
17. L. E. KAY, D. A. TORCHIA, AND A. BAX, *Biochemistry* **28,** 8972 (1989).
18. J. CAVANAGH, A. G. PALMER, P. E. WRIGHT, AND M. RANCE, *J. Magn. Reson.* **91,** 429 (1991).
19. G. BODENHAUSEN AND D. J. RUBEN, *Chem. Phys. Lett.* **69,** 185 (1980).
20. L. MÜLLER, *J. Am. Chem. Soc.* **101,** 760 (1979).
21. M. R. BENDALL, D. T. PEGG, AND D. M. DODDRELL, *J. Magn. Reson.* **52,** 81 (1983).

22. A. BAX, R. H. GRIFFEY, AND B. L. HAWKINS, *J. Magn. Reson.* **55,** 301 (1983).
23. A. G. REDFIELD, *Chem. Phys. Lett.* **96,** 537 (1983).
24. E. R. P. ZUIDERWEG, *J. Magn. Reson.* **86,** 346 (1990).
25. G. A. MORRIS AND R. FREEMAN, *J. Am. Chem. Soc.* **101,** 760 (1979).
26. O. W. SØRENSEN, G. EICH, M. H. LEVITT, G. BODENHAUSEN, AND R. R. ERNST, *Prog. NMR. Spectrosc.* **16,** 163 (1983).
27. A. BAX, M. IKURA, L. E. KAY, D. A. TORCHIA, AND R. TSCHUDIN, *J. Magn. Reson.* **86,** 304 (1990).
28. (*a*) T. J. NORWOOD, J. BOYD, J. E. HERITAGE, N. SOFFE, AND I. D. CAMPBELL, *J. Magn. Reson.* **87,** 488 (1990); (*b*) T. J. NORWOOD, J. BOYD, AND I. D. CAMPBELL, *FEBS Lett.* **255,** 369 (1989).
29. J. KEELER AND D. NEUHAUS, *J. Magn. Reson.* **63,** 454 (1985).
30. J. CAVANAGH AND M. RANCE, *J. Magn. Reson.* **88,** 72 (1990).
31. A. ABRAGAM, "The Principles of Nuclear Magnetism," pp. 289–300, Oxford Univ. Press, Oxford, 1961.
32. R. R. ERNST, G. BODENHAUSEN, AND A. WOKAUN, "Principles of NMR in One and Two Dimensions," p. 504, Clarendon, Oxford, 1987.
33. A. BAX, L. E. KAY, S. W. SPARKS, AND D. A. TORCHIA, *J. Am. Chem. Soc.* **111,** 408 (1989).
34. R. RICHARZ, K. NAGAYAMA, AND K. WÜTHRICH, *Biochemistry* **19,** 5189 (1980).
35. G. WAGNER, *Q. Rev. Biophys.* **16,** 1 (1983).
36. A. J. SHAKA, J. KEELER, T. FRENKIEL, AND R. FREEMAN, *J. Magn. Reson.* **52,** 335 (1983).
37. D. MARION AND K. WÜTHRICH, *Biochem. Biophys. Res. Commun.* **113,** 967 (1983).
38. L. MÜLLER AND R. R. ERNST, *Mol. Phys.* **38,** 963 (1979).
39. J. CAVANAGH AND J. KEELER, *J. Magn. Reson.* **77,** 356 (1988).
40. G. BODENHAUSEN, R. FREEMAN, AND D. L. TURNER, *J. Magn. Reson.* **27,** 511 (1977).
41. D. H. LIVE, D. G. DAVIS, W. C. AGOSTA, AND D. J. COWBURN, *J. Am. Chem. Soc.* **106,** 1939 (1984).
42. (*a*) J. GLUSHKA, M. LEE, S. COFFIN, AND D. J. COWBURN, *J. Am. Chem. Soc.* **111,** 7716 (1989); (*b*) J. GLUSHKA, M. LEE, S. COFFIN, AND D. J. COWBURN, *J. Am. Chem. Soc.* **112,** 2843 (1990).